# Chaotic effects in IR resonant molecular vibrational photodesorption

G. P. Brivio
*Dipartimento di Fisica, Università di Milano, Via Celoria 16, 20133 Milano, Italy*

M. Torri
*Dipartimento di Fisica, Università di Trieste, Via Valerio 2, 34127 Trieste, Italy*
*and Dipartimento di Fisica, Università di Milano, Via Celoria 16, 20133 Milano, Italy*
(Received 1 April 1993)

In this paper the process of IR resonant molecular vibrational photodesorption, applied to the system $CH_3F$-NaCl, is treated in terms of a simple two-dimensional (2D) classical model. Desorbing trajectories are shown to undergo a chaotic motion. By using the transport theory in Hamiltonian systems, in the phase space spanned by the coordinates of molecule-surface bond (the other coordinate being the intramolecular vibrational excitation), the characteristic bottlenecks, which render IR photodesorption an infrequent event, are located, the rates through them are computed, and the time evolution of the system is followed up to all times. A comparison with results obtained from numerical simulations, which are shown to be impractical in most of the cases of physical interest, is presented.

## I. INTRODUCTION

A detailed microscopic description of desorption processes of molecules from solid surfaces is useful in several respects. For example, it can clarify the role of the energy-transfer mechanism, both the intramolecular one and that between the adsorbate and the solid, and unravel the existence of bottlenecks which may render such a phenomenon an infrequent event. In this field, it is particularly interesting to investigate selective desorption processes, i.e., those where an external probe excites one of the intramolecular (electronic or vibrational) degrees of freedom of the adsorbate.[1–4] While the system relaxes into a new configuration, an energy exchange between various degrees of freedom can occur leading to desorption of molecules from the surface. In the theoretical treatment of desorption induced by electronic transitions (DIET),[5] the interaction between the adsorbate and the substrate phonons is usually ignored since the time scale of the process is very short; in IR-resonant molecular vibrational photodesorption (IR-RMVP), where one resonantly excites an intramolecular vibration, the validity of such an approximation seems to be controversial even at very low substrate temperatures, and in any case, it strongly depends on the system under investigation.[6–8]

It is well known that a correct description of an IR-RVMP process stems from quantum mechanics[9] and wave-packet calculations for the molecular motion have been performed.[10] However, correct desorption times, often much longer than picoseconds, cannot be presently achieved in this way because of computational limitations. Since interesting information on molecule-surface interaction can also be obtained by classical mechanics for models with few degrees of freedom, such a solution for IR-RMVP is still worthwhile,[11–14] especially in view of the information that can be obtained by using recently developed methods of stochastic mechanics.[15,16] They are particularly powerful for two-dimensional (2D) Hamiltonian systems allowing one to locate bottlenecks in phase space which hamper energy transfer in physical systems, and to calculate the relevant rates of the process under investigation.[17,18]

In this paper we shall apply the transport theory in Hamiltonian systems (TTHS) to the elastic resonant state decay (ERSD) model, whose application to IR-RVMP, has been extensively investigated.[4,14] This model consists of a Hamiltonian with two nonlinearly coupled degrees of freedom, one being the intramolecular vibration pumped by the IR radiation, the other the molecule-surface bond. When the former is excited up to an energy greater than the depth of the adsorption potential, then the energy relaxation due to the nonlinear coupling between the two oscillators may lead to desorption. In Ref. 14 such a model has been studied by integrating the classical equations of motion to obtain the desorption rate by suitably averaging over a set of initial conditions, and to analyze the phase-space structure of the system in terms of the Poincaré sections. From such an analysis applied to IR-RMVP of $CH_3F$ physisorbed on NaCl,[6] a qualitative explanation has been given why the survival probability of the molecule in an adsorbed state does not follow a single exponential decay law. Here we wish to proceed further by exploiting the properties of nonlinear classical Hamiltonian mechanics in order to locate the relevant bottlenecks in an IR-RMVP process and to compute the rates through them and the evolution of the system using TTHS methods. It is worthwhile to point out that such methods have already been used in the vibrational predissociation of van der Waals molecules.[17,18] Yet, the ERSD model applied to an IR-RMVP process such as $CH_3F$ desorption from NaCl, although described by essentially the same Hamiltonian, displays the follow-

 

ing peculiar features that make it different from vibrational predissociation of molecules such as He-$I_2$, and warrant a separate investigation:[6,9,19] (i) the depth $V_0$ of the physisorption potential is much larger than that of the van der Waals potential between He and $I_2$; (ii) $V_0 > \hbar\omega_H$, $\omega_H$ being the frequency associated with the intramolecular C-F stretching mode $\nu_3$ excited by the IR radiation; (iii) the mismatch of the two fundamental frequencies $\omega_H$ and $\omega_0$ for the van der Waals bond is much larger for $CH_3F$-NaCl than for He-$I_2$. In fact, these properties imply that the process to release $CH_3F$ from NaCl takes a few orders of magnitude longer than that to dissociate He from $I_2$. This reflects a much more complex phase-space structure for the former system closely related to the infrequent event character of IR-RMVP. Also, in a perturbative quantum calculation, one observes a five order of magnitude jump of the desorption rate of $CH_3F$ from NaCl, as a function of the physisorption bond energy,[14] not to be found in the vibrational predissociation of van der Waals molecules such as He-$I_2$.[20]

In Sec. II we present the main equations of the ERSD model, in Sec. III we discuss the method to locate the intramolecular and desorption bottlenecks and to calculate the rates through them. In Sec. IV the time evolution of the system for different sets of initial conditions is presented. The conclusions in Sec. V point out that the IR-RMVP process is an example of molecule-surface interaction where the desorbing trajectories display chaotic motion.[21–23]

## II. BASIC EQUATION OF THE ELASTIC RESONANCE STATE DECAY MODEL

IR resonant molecular vibrational photodesorption (IR-RMVP) is a process of quantum nature, which may occur after an intramolecular vibrational mode of the physisorbed molecule is resonantly promoted to an excited state by absorbing one or more photons of the IR laser radiation. If such a state is degenerate with continuum states of the molecule-surface potential, then a resonance state decay may lead to desorption, while the intramolecular vibration is simultaneously deexcited. This process is called an elastic resonance state decay (ERSD), when the energy, initially deposited by the laser in the intramolecular vibration, is conserved within the molecule-inert solid system (i.e., no energy is exchanged with the phonons of the solid). The details and the limitations of the ERSD model to describe IR-RMVP are discussed in Refs. 4 and 14.

In practice the Hamiltonian $H$ of the ERSD model considers a 2D linear molecule physisorbed orthogonal to the surface. It can be written as

$$H = H_0 + \Delta H, \tag{1}$$

$$H_0 = H_V + H_M, \tag{2}$$

$$H_V = \frac{p_x^2}{2m} + \frac{1}{2}mw(x - x_0)^2, \tag{3}$$

$$H_M = \frac{p_y^2}{2} + \exp[-2(y - \sigma x_0)] - 2\exp[-(y - \sigma x_0)], \tag{4}$$

$$\Delta H = \exp[-2(y - \sigma x)] - 2\exp[-(y - \sigma x)] - \exp[-2(y - \sigma x_0)] + 2\exp[-(y - \sigma x_0)]. \tag{5}$$

Note that Eqs. (3), (4), and (5) are expressed in suitable dimensionless units defined, as well as the parameters $m$, $w$, and $\sigma$, in Ref. 14. The Hamiltonian $H_V$ describes the intramolecular degree of freedom in terms of a harmonic oscillator of frequency $\omega_H$. The Hamiltonian $H_M + \Delta H$ describes the surface van der Waals bond approximated by a Morse potential which is nonlinearly coupled to the harmonic vibration. $(x, p_x)$ and $(y, p_y)$ are the canonical coordinates and momenta for the harmonic and the van der Waals motion, respectively, and $\omega_0$ the frequency at the bottom of the Morse potential of depth $V_0$, when the harmonic oscillator is at the equilibrium position $x = x_0$. More generally, it is a function of $\epsilon_M$ to be labeled as $\omega_M(\epsilon_M)$. Say $\tau$ and $\epsilon$ are the dimensionless times and energies, respectively, and recall that the corresponding dimensional times $t$ and energies $E$ are $t = \sqrt{2}/\omega_0\tau$ and $E = \epsilon\, V_0$, respectively. In Table I the values of $V_0$, $\omega_0$, and $\omega_H$ for the system $CH_3F$-NaCl are shown.

The system is allowed to evolve in time following the classical Hamiltonian equations of motion. However, owing to the quantum character of IR-RVMP and hence following a previous treatment which allowed a comparison between the classical and the quantum perturbative desorption rates, the initial conditions are fixed as follows. First, one assumes that the total energy $\epsilon$ is (approximatively) shared between the two unperturbed oscillators,[14] so that it can be split between the two eigenvalues of $H_V$ and $H_M$, $\epsilon^v$ and $\epsilon_j$, respectively, corresponding to the eigenstate $|vj\rangle \equiv |v\rangle \otimes |j\rangle$,

$$(H_V + H_M)|vj\rangle = (\epsilon^v + \epsilon_j)|v\rangle|j\rangle. \tag{6}$$

Second, the two remaining initial conditions are chosen among two sets of coordinates, one for each bond, allowed by the previous conditions, and equally distributed in time over a period of both oscillators, say $T_H$ and $T_M$ for the harmonic and the van der Waals bond, respectively. Energies are chosen in such a way that $\epsilon^v > 0$ always, and $\epsilon_j < 0$ for bound states in the molecule-surface motion. A necessary condition for desorption is then $\epsilon^v + \epsilon_j > 0$. One can calculate the desorption probability $P(\tau)$ by integrating the Hamilton equations of motion starting from a suitably large set of initial conditions. Details are discussed in Ref. 14.

One of the main results of Ref. 14 for IR-RMVP applied to $CH_3F$-NaCl is that the survival probability $1 - P(\tau)$ can be approximately fitted with two exponential decay laws, one at a shorter and one at a longer time. The latter allows one to introduce a desorption rate, say $\mu_{1,\text{class}}$ due to slow desorbing trajectories, and the former

TABLE I. Characteristic parameters for the system $CH_3F$/NaCl.

| $V_0$ meV | $\omega_0$ ($s^{-1}$) | $\omega_H$ ($s^{-1}$) |
|---|---|---|
| 233 | $3.28 \times 10^{13}$ | $1.82 \times 10^{14}$ |

a rate $\mu_{2,\text{class}}$ due to fast desorbing ones. The scope of this paper is to use the transport theory in Hamiltonian system (TTHS) methods in order to obtain a more accurate and more insightful description of the time evolution of the desorbing system, and a comparison of the results with those obtained by numerical simulations, when available.

## III. PHASE-SPACE PROPERTIES AND DESORPTION BOTTLENECKS

In order to investigate the classical phase-space structure and relate it to the desorption process for the ERSD model, a 2D conservative system, the most convenient way is to make use of the Poincaré section in a plane spanned by the coordinates and momenta $(y, p_y)$ of the van der Waals motion. In a $(y, p_y)$ Poincaré section, the point $[y(\tau), p_y(\tau)]$ is recorded in that plane for a given classical trajectory for such $\tau$'s for which $x(\tau) = x_0$, provided $p_x > 0$. It is useful to start our analysis by showing the Poincaré section in Fig. 1 obtained with initial energies $\epsilon_{j=0}$, $\epsilon^{v=20}$ [to be denoted $(j = 0, v = 20)$ henceforth] for $N = 50$ trajectories integrated up to the time $\tau = 3000$. A magnified portion of Fig. 1, to be discussed in the following, is shown in Fig. 2. Although such a high excitation of the molecular vibration cannot be achieved experimentally, nevertheless this is a simple and instructive case to show how to use the TTHS to locate the characteristic bottlenecks and calculate the rates through them. In such a Poincaré section, one observes an inner region with regular motion and a more external one where the motion is chaotic. One also verifies that the stochastic trajectories are the desorbing ones. The regular region is occupied by closed curves called invariant tori, slightly perturbed by the nonlinear coupling between the two oscillators, and by smaller closed curves, called islands, around the points representing resonances between the two motions. Observing that the

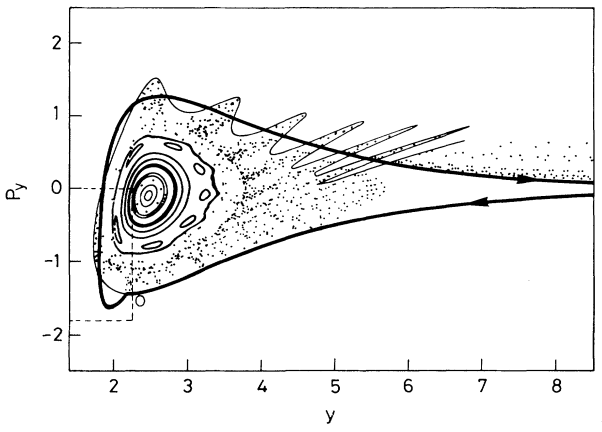


FIG. 1. The Poincaré section for $\epsilon = \epsilon^{v=20} + \epsilon_{j=0}$ and $N = 50$ trajectories. The two contours going to zero for $y \to \infty$ and joining at the point $O$ are the desorption separatrix. Desorbing trajectories are contained within the flux-out area of its homoclinic oscillations.

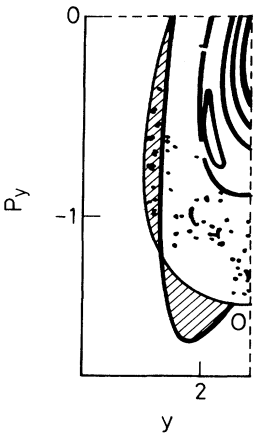


FIG. 2. The shaded eight-shaped area is the magnified turnstile from Fig. 1.

nonlinear coupling between the two degrees of freedom is not too strong in the island region, the resonances approximately occur when the ratio between the frequencies of the two unperturbed oscillators is a rational number: $\omega_H/\omega_M(\epsilon_M) = n/m$. For our parametrization of the ERSD model the resonance with the smallest ratio is the $(n = 6, m = 1)$ seen in Fig. 1 as six tiny islands surrounding the two innermost shown invariant tori. The last regular structure seen in Fig. 1 refers to the $(7, 1)$ resonance. Recall that two cycles are associated to any $(n, m)$ resonance: a stable one formed by elliptic points centered within the islands (seen in Fig. 1) and an unstable one formed by hyperbolic points $\mathcal{H}_{n,m}$, joined by a separatrix (see the Poincaré-Birkhoff theorem).[24] Stochastic regions generally exist in the neighborhood of the separatrix. On such a Poincaré section take two ensembles of trajectories, e.g., a set of points lying on two segments, either of them starting from two adjacient hyperbolic points, one belonging to the the stable and the other to the unstable branch of the separatrix, as in Ref. 17. Propagate the points on the stable and unstable branches backward and forward in time, respectively, until the two branches intersect for the first time at a homoclinic point. The closed curve formed in this way by the stable and unstable branches of the hyperbolic points of the corresponding cycle $\mathcal{H}_{n,m}$ is called a dividing surface. One more forward propagation of such a curve through the Poincaré section determines a curve identical to the dividing surface, except in the neighborhood of the homoclinic point. If we superimpose this new curve upon the old one, the difference between them is just an eight-shaped figure, which is often called turnstile. In fact, while the just-mentioned forward propagation of the stable branch leaves a gap in the neighborhood of the first homoclinic point, the same propagation of the unstable branch moves away from the dividing surface and fills such a gap with a curve having an oscillatory character. By further propagating forward in time the unstable branch, this crosses the stable branch of the dividing surface infinitely many times. The intersections are called homoclinic points, and the oscillations homoclinic ones. In this way the turnstile is

constituted by the first two homoclinic oscillations of the unstable branch. An example of homoclinic oscillations, associated with the (7,1) resonance, is shown in Fig. 3. Recall that any separatrix defines two dividing surfaces, since at any hyperbolic point four curves (two incoming branches and two outgoing ones) join Ref. 25. We shall take into account that dividing surface, which is defined more exactly in Appendix A. Because the ERSD system is conservative, the area contained within any homoclinic oscillations is preserved, as a consequence of the Liouville theorem. The properties of any unstable cycle, together with the generation of the turnstile for a similar system, are shown in Ref. 17. Here we only recall that, in the phase space spanned by the canonical coordinates of the van der Waals motion, half of the area of the turnstile lying outside the dividing surface is called the flux out and the other half, lying inside it, the flux into the region surrounded by the separatrix.[16] Since, for any unstable cycle, trajectories cross the separatrices only through the corresponding turnstiles, such separatrices indeed constitute the dynamical *intramolecular* bottlenecks for the motion of the van der Waals bond. It has been shown that the last invariant torus to disappear in the standard map is the one characterized by a ratio $\omega_H/\omega_M = 1+\gamma_g$, with $\gamma_g = \frac{\sqrt{5}-1}{2}$, the golden mean.[26] More recent work in molecular physics has focused attention on similar tori, characterized by a ratio $\omega_H/\omega_M = r + \gamma_g$ ($r$ real), as the strongest invariant tori to break, although they are not generally the last ones to disappear.[17] The remnants of such tori, partially destroyed by the nonlinear coupling between the two oscillators, are invariant Cantor sets which represent the most important bottlenecks also for the ERSD system. In fact, they constitute strong barriers to the stochastic motion. The first cantorus displaying the character of an intramolecular bottleneck, for our parametrization of the ERSD model, corresponds

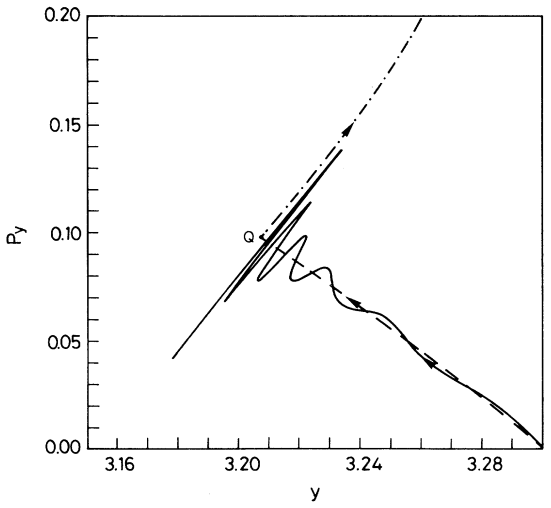


FIG. 3. The Poincaré section for $\epsilon = \epsilon^{v=20} + \epsilon_{j=0}$ near a hyperbolic point **Q** for the resonance (7,1). The dashed line is one of its two stable branches and the dotted-dashed line is one of its two unstable branches. The solid line is one of the unstable branches of the neighboring hyperbolic point.

to $r = 7$. By expanding the irrational number $7 + \gamma_g$ into continuous fractions, one obtains the convergents $\mathcal{C}_{n,m} = \{(7,1), (8,1), (15,2), (23,3), \ldots\}$, each of them characterized by a frequency ratio $\omega_H/\omega_0 = n/m$, which approximate the ratio $7 + \gamma_g$ better and better. Since a continuous-fraction expansion converges very rapidly, few convergents $\mathcal{C}_{n,m}$ are enough to obtain an unstable cycle, which well approximates the properties of the corresponding cantorus. In particular, one can often calculate the flux in and the flux out and the corresponding *rates in* and *rates out* (see Appendix B) through such a bottleneck with very good accuracy, by using the area of the turnstile of the separatrix of the first convergent.

There is also another important bottleneck in the system: the one which all trajectories leading to desorption must pass through. In Fig. 1 the two contours (in bold face) going to zero for $y \to \infty$ and joining at the point $O$ are defined as the *desorption* separatrix between the bound and the unbound motion for the van der Waals degree of freedom. This separatrix has only one (degenerate) hyperbolic point for $y \to \infty$. After propagating in time an ensemble of trajectories from the hyperbolic point forward for negative $p_y$ (unstable branch) and backward for positive $p_y$ (stable branch), the two intersect at the homoclinic point $O$ for the first time (Fig. 1). These branches, i.e., the thicker curve in Fig. 1, form the desorption separatrix. Further forward propagation of the unstable branch past the point $O$ leads to several homoclinic oscillations. The first eight-shaped figure, which is magnified in Fig. 2, represents the turnstile associated with the desorption separatrix. Note that all desorbing trajectories are contained only within those regions of the homoclinic oscillations which lie outside the desorption separatrix. In conclusion, both the desorption and the intramolecular separatrices are the relevant bottlenecks for the ERSD model.

In order to calculate the time evolution of our system in terms of the flux in and out areas of the turnstiles, we need the following.

(i) A definition of the rate through any turnstile, e.g., the frequency by which an ensemble of trajectories crosses a bottleneck. These rates will be denoted by $\lambda_{i,i+1}$ (when they refer to the transport rate from an inner $R_i$ to an outer $R_{i+1}$ region), and by $\lambda_{i+1,i}$, in the opposite case. In both cases, $0 \le i \le s$. In short, the former will be called *rates out*, the latter *rates in*. They are defined in Appendix B. Of course $\lambda_{s,s+1}$ is the last *rate out* leading to desorption. The rates $\lambda_{i,j}$ form a real nonsymmetric matrix, with a null diagonal element. An accurate definition of any region $R_i$ is given in Appendix A.

(ii) A method of fundamental, although technical, relevance, namely how to very accurately locate the hyperbolic points of any unstable cycle $\mathcal{H}_{n,m}$. In fact, only a very accurate estimate ($\mathbf{Q}'$) of the hyperbolic points ($\mathbf{Q}$) can result in a correct identification of the stable and unstable branches of the separatrix. In practice, the following condition is required: $10^{-9} < |\mathbf{Q}' - \mathbf{Q}| < 10^{-10}$ in the dimensionless units defined in Ref. 14. The method for finding **Q** is given in Appendix C.

Then we assume that in each region except the regular

one, which never contributes to desorption, the motion is completely chaotic, so that a system of first-order kinetic equations is appropriate to describe the dynamics of the desorbing trajectories.[18]

$$\begin{aligned}\frac{dN_0(\tau)}{d\tau} &= -\lambda_{(0,1)}N_0 + \lambda_{(1,0)}N_1,\\ \frac{dN_i(\tau)}{d\tau} &= -\lambda_{(i,i-1)}N_i - \lambda_{(i,i+1)}N_i + \lambda_{(i-1,i)}N_{i-1}\\ &\quad +\lambda_{(i+1,i)}N_{i+1},\\ \frac{dN_s(\tau)}{d\tau} &= -\lambda_{(s,s+1)}N_s - \lambda_{(s,s-1)}N_s + \lambda_{(s-1,s)}N_{s-1}. \quad (7)\end{aligned}$$

This system of $(s+1)$ equations implies that the phase space leading to desorption can be subdivided into $(s+1)$ subregions, so that a trajectory starting from the innermost one ($s=0$) has to cross $(s+1)$ bottlenecks before desorbing. $N_i$ are the trajectories within the $i$th stochastic region, with $0 \le i \le s$. We can recast the system (7) in the matrix form

$$\dot{\mathbf{n}} = \mathbf{\Lambda}\dot{\mathbf{n}}, \quad (8)$$

where $\boldsymbol{n}$ is a column vector whose elements are $n_i = N_i/N$ ($N$ is the total number of trajectories) and $\mathbf{\Lambda}$ is a square nonsymmetric matrix whose elements can be worked out in terms of the rates $\lambda_{i,j}$ defined above. The solution of Eq. (8) is[4]

$$n_i(t) = \sum_j A_j(i)\exp(-\mu_j\tau), \quad (9)$$

$$A_j(i) = a_j(i)\sum_{i'} b_j(i')n_{i'}(\tau=0), \quad (10)$$

where $\mu_j$ are the (non-negative) eigenvalues of $-\mathbf{\Lambda}$ and $\boldsymbol{a}_j$ and $\boldsymbol{b}_j$ are the corresponding right and left eigenvectors. The survival probability $S(\tau)$ can be expressed in terms of the solutions (9) of the system (7), as

$$S(\tau) = \bar{n} + \sum_0^s n_i(\tau), \quad (11)$$

with $\bar{n} = \bar{N}/N$ and $\bar{N}$ is the total number of regular trajectories that never desorb.

At this point it is crucial to select the unstable cycles $\mathcal{H}_{n,m}$ of the strongest intramolecular bottlenecks of our system. When a lot of trajectories are stochastic, as in the case $(j=0, v=20)$, they are given by the convergents $\mathcal{C}_{n,m}$ of the cantori. So we calculate the rates through the corresponding turnstiles, and by Eq. (11) compute $S(\tau)$, which can be also compared with $1-P(\tau)$ obtained with a numerical simulation. In other cases, most of the initial conditions may refer to regular trajectories, so that the initial conditions leading to stochastic motion could be much inside any cantorus. In such a case the first innermost stochastic region $R_0$ (see Appendix A) is just a narrow strip between the last regular torus and the separatrix of the unstable cycle of a resonance which may not be the convergent of any cantorus.

## IV. RESULTS

We wish to calculate the survival probability $S(\tau)$ for the ERSD model, parametrized in such a way as to describe IR-RMVP for the system $CH_3F$-NaCl,[14] using the TTHS. This theory allows one to calculate the dynamical behavior of the system, without integrating a suitable set of initial conditions for long times and then averaging over them, as is usually done in numerical simulations. This fact turns out to be crucial in the analysis of photodesorption of $CH_3F$ physisorbed on NaCl, since the process is infrequent in character. Consequently, a numerical simulation becomes often an impractical tool to be used for determining realistic desorption rates, especially when the total energy of the system is hardly higher than the threshold energy of the physisorption bond. This is indeed the experimental situation,[6] where the intramolecular stretching bond C—F ($\nu_3$) of the $CH_3F$ molecule is unlikely be excited up to a level higher than $v=2$ because of its anharmonicity. It would be natural to investigate the case $(j=0, v=2)$, since at ambient temperature, the state with $\epsilon_{j=0}$ has the greatest occupancy. However, for such a splitting, $\epsilon = \epsilon_{j=0} + \epsilon^{v=2}$, of the total energy, the system is regular and no desorption occurs.

We present results for the time evolution of the system for the following three initial energy partitions: $(j=0, v=20)$, $(j=2, v=2)$, and $(j=1, v=2)$. The two latter ones are physically more significant and represent the hardest test for our parametrization. For $(j=0, v=20)$ one can easily obtain numerically $1-P(\tau)$ by integrating the classical equations of motion, because the internal relaxation of the system is fast, desorption occurs on a shorter time scale, and there is good statistics of desorbing trajectories. From a detailed analysis of the Poincaré section in Fig. 1, we see that the convergent $\mathcal{C}_{(7,1)}$, of the cantorus deriving from the breaking of the torus characterized by a ratio $\omega_H/\omega_M = 7+\gamma_g$ is the only important intramolecular bottleneck. So, it suffices to subdivide the stochastic region into two parts: the first one between the inner regular region and $\sigma_0(7,1)$ and a second one between $\sigma_0(7,1)$ and the desorption separatrix. Note that here we can neglect the rate into the region limited by $\sigma_0(7,1)$, because it is much smaller than the rates out. Figure 4 shows the survival probabilities $S(\tau)$ and $1-P(\tau)$. The two curves are in very good agreement. We note that at short times $1-P(\tau)$ is lower than $S(\tau)$, because some trajectories immediately desorb within one period of the harmonic oscillator $T_H$. At longer times, the situation is reversed, since only one intramolecular bottleneck ($\mathcal{C}_{(7,1)}$) approximates the dynamical effect of the cantorus. It is interesting to compare the rates, $\mu_{1,\mathrm{class}}$ and $\mu_{2,\mathrm{class}}$, obtained by the best fit of $1-P(\tau)$ with two exponentially decaying functions, with the two eigenvalues of Eq. (8), for this case. Their values are reported in Fig. 4. While qualitatively both results show the existence of two characteristic times, e.g., the inverse of such rates [see Eqs. (9)–(11)], the eigenvalues are about one order of magnitude larger than the rates of the fit. However, $S(\tau)$ reproduces much better $1-P(\tau)$ than the numerical fit reported in Ref. 14.

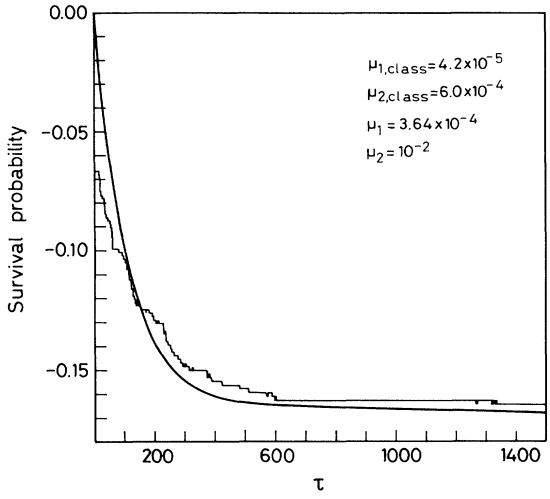


FIG. 4. Plot of $\log_{10}[1 - P(\tau)]$ for $(j = 0, v = 20)$ using $N = 400$ trajectories (bumpy line), and $\log_{10}[S(\tau)]$ (solid line). For the values of $\mu$ see the text.

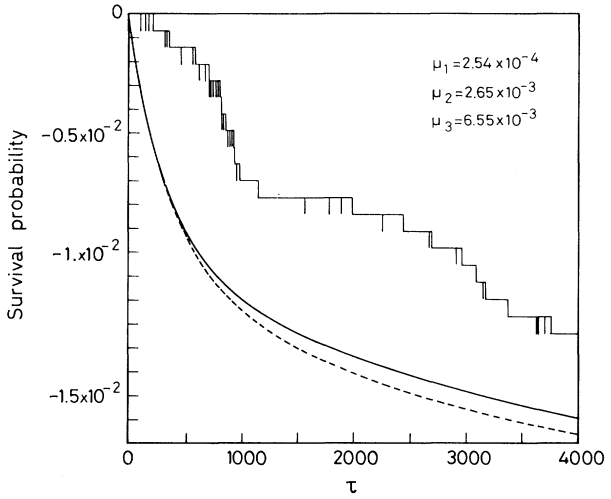


FIG. 5. Plot of $\log_{10}[1 - P(\tau)]$ for $(j = 2, v = 2)$ using $N = 500$ trajectories (bumpy line), and $\log_{10}[S(\tau)]$ (solid line). The broken line represents $\log_{10}[S(\tau)]$ without the rate in. For the values of $\mu$ see the text.

One reason is that here in Eq. (11), we have taken into account a term $\bar{n}$ representing the regular trajectories. More generally, the calculated $S(\tau)$ confirms the validity of the TTHS applied to this problem.

Both the cases $(j = 1, v = 2)$ and $(j = 2, v = 2)$ show Poincaré sections where the regular regions are enhanced for the nonlinear coupling between the two oscillators is smaller than for $(j = 0, v = 20)$. This is related to a stronger dynamical effect of the various bottlenecks. Here more than one intramolecular bottleneck has to be taken into account and the contribution of the rates in to the time behavior of the system cannot be neglected. For $(j = 2, v = 2)$, the cantorus deriving from the breaking of the torus $7 + \gamma_g$ determines the strongest bottleneck, and the convergent $\mathcal{C}_{(8,1)}$ well approximates its dynamical effect. Also the bottleneck associated with the resonance $(17, 2)$, which is the second convergent of the cantorus $8 + \gamma_g$, plays an important role in the dynamics of the system. So in this case we have taken into account three stochastic regions: the first one surrounded by the last regular torus and $\sigma_0(8, 1)$, the second in between $\sigma_0(8, 1)$ and $\sigma_1(17, 2)$, and the third in between $\sigma_1(17, 2)$ and the desorption separatrix. Figure 5 shows the comparison between $S(\tau)$ and $1 - P(\tau)$. The broken line is obtained neglecting the rate in $\lambda_{1,0}$, while $\lambda_{1,2}$ is always negligible. When we include $\lambda_{1,0}$, the survival probability $S(\tau)$ increases slightly. From Fig. 5 we observe that one eigenvalue of Eq. (8) is much smaller than the others, so determining the long-time behavior of the system. $1 - P(\tau)$ in Fig. 5 has been obtained by a numerical simulation integrating a set of 500 initial conditions up to a time $\tau = 4000$, although with rather poor statistics of desorbing trajectories ($\sim 3\%$). Calculations for longer times are impractical so that it is dubious how to extract basic information on the ERSD process for IR-RMVP from any simulation.

The numerical difficulties involved in the case $(j = 2, v = 2)$ increase for $(j = 1, v = 2)$. Stochastic, eventually desorbing trajectories are indeed a very small fraction of the total number of trajectories constituting the statistical ensemble of the system ($\sim 0.25\%$). All the desorbing trajectories start in the stochastic layer surrounded by the separatrix $\sigma_0(31, 4)$. This is the strongest bottleneck for the system, although it is not a convergent of any cantorus, because all stochastic, eventually desorbing, trajectories are included within a very narrow strip determined by the last regular torus and $\sigma_0(31, 4)$. The phase space in the region of two adjacent hyperbolic points for the resonance $(31, 4)$ is shown in Fig. 6. The dynamical effect of the cantorus $8+\gamma_g$ is important and it is well described by the separatrix of its first convergent $\mathcal{C}_{(8,1)}$. So two more stochastic regions have been taken into account: that in between $\sigma_0(31, 4)$ and $\sigma_1(8, 1)$ together with the region outside $\sigma_1(8, 1)$ bounded by the

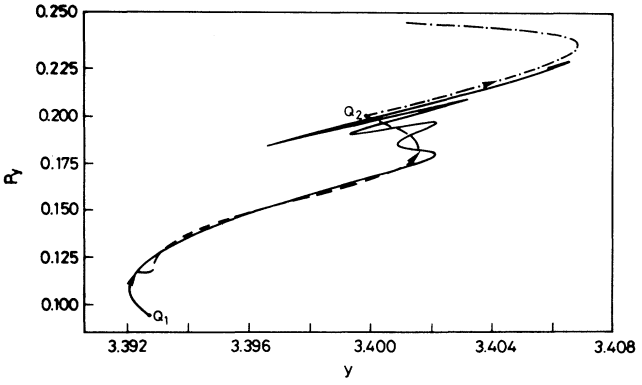


FIG. 6. The Poincaré section for $\epsilon = \epsilon^{v=2} + \epsilon_{j=1}$ in the region of two adjacent hyperbolic points $\mathbf{Q}_1$ and $\mathbf{Q}_2$ for the resonance $(31, 4)$. For details see Fig. 3.

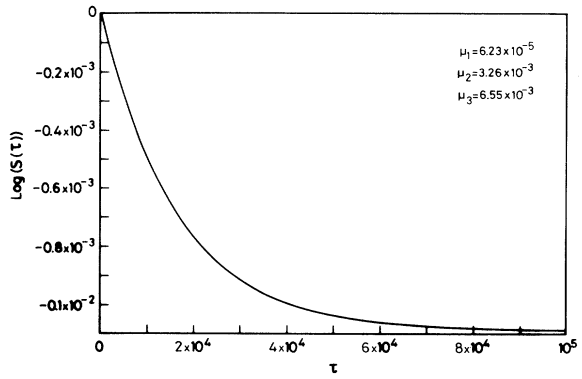


FIG. 7. Plot of $\log_{10}[S(\tau)]$ for $(j = 1, v = 2)$. For the values of $\mu$ see the text.

desorption separatrix. In Table II all details for the case $(j = 1, v = 2)$ are summarized. Observe that the rate in $\lambda_{2,1}$ is not included, being negligible as in the previous case. Similarly (see Fig. 7 ) there is a much smaller eigenvalue determining the long-time behavior of the system so that all trajectories desorb in about $10^{-9}$s, roughly the inverse of $\mu_1$. In Fig. 7 the behavior of $S(\tau)$ is shown. No significant results can be obtained by a numerical simulation.

## V. CONCLUSIONS

This work contributes to two aspects of the molecule-surface interaction. First, it shows that desorbing trajectories undergo a chaotic motion and that by using the techniques of stochastic mechanics such as the TTHS, it is possible to handle the time behavior of a molecule-surface interacting system characterized by the fact of being an infrequent event, such as IR-RMVP. Table II shows that for the initial condition $(j = 1, v = 2)$, out of $10^4$ initial trajectories only 0.25% are stochastic ones, eventually desorbing. In such a case, while a classical simulation has very little meaning, since the statistics of the desorbing trajectories is extremely poor (consider that we could not follow a single one up to desorption for $\tau = 10^4$), the TTHS allows one to obtain the time behavior of the ERSD model parametrized to describe $CH_3F$ desorbing from NaCl. For such a system we have been able to compute relevant rates down to $10^8$ $s^{-1}$, but smaller ones could be obtained for other similar systems with the same method. In conclusion, the TTHS allows for a clear identification in the phase space of the physical bottlenecks, and provides a method to compute the rates through them independently of any simulation.

Second, looking at the very low percentage of desorbing trajectories from the van der Waals state $(j = 1, v = 2)$, whose population is much smaller than that of the

TABLE II. Phase-space region and rates for the case $(j = 1, v = 2)$. A sample of $N = 10^4$ initial conditions is considered.

| | | | |
|---|---|---|---|
| AREA of the inner regular region | $(A_r)$ | = | 2.63 |
| AREA of the region enclosed by the separatrix $\sigma_0(31,4)$ | $(A_{s,0})$ | = | 2.70 |
| AREA of the region enclosed by the separatrix $\sigma_1(8,1)$ | $(A_{s,1})$ | = | 3.405 |
| AREA of the region enclosed by the desorption separatrix | $(A_{s,2})$ | = | 8.88 |
| AREA of the quasiperiodic region for the resonance $(31,4)$ | $(A_{qp,0})$ | = | 0.00 |
| AREA of the quasiperiodic region for the resonance $(1,8)$ | $(A_{qp,1})$ | = | 0.174 |
| AREA of the stochastic region $R_0$ | $(A_0 = A_{s,0} - A_r - A_{qp,0})$ | = | 0.07 |
| AREA of the stochastic region $R_1$ | $(A_1 = A_{s,1} - A_{s,0} - A_{qp,1} - A_{qp,0})$ | = | 0.53 |
| AREA of the stochastic region $R_2$ | $(A_2 = A_{s,2} - A_{s,1})$ | = | 5.475 |
| AREA of the flux out associated with the turnstile of $R_0$ | $(A_{t,0})$ | = | $3.5\times10^{-6}$ |
| AREA of the flux out associated with the turnstile of $R_1$ | $(A_{t,1})$ | = | $1.4\times10^{-3}$ |
| AREA of the flux out associated with the turnstile of $R_2$ | $(A_{t,2})$ | = | $2.87\times10^{-2}$ |
| RATE in the region $R_0$ | $[\lambda_{(1,0)} = A_{t,0}/(A_1 T_H)]$ $(s^{-1})$ | = | $8.25\times10^{-6}$ |
| | | = | $1.9\times10^{8}$ |
| RATE out the region $R_0$ | $[\lambda_{(0,1)} = A_{t,0}/(A_0 T_H)]$ $(s^{-1})$ | = | $6.25\times10^{-5}$ |
| | | = | $1.45\times10^{9}$ |
| RATE out the region $R_1$ | $[\lambda_{(1,2)} = A_{t,1}/(A_1 T_H)]$ $(s^{-1})$ | = | $3.25\times10^{-3}$ |
| | | = | $7.54\times10^{10}$ |
| RATE out the region $R_2$ | $[\lambda_{(2,3)} = A_{t,2}/(A_2 T_H)]$ $(s^{-1})$ | = | $6.55\times10^{-3}$ |
| | | = | $1.52\times10^{11}$ |
| NUMBER of trajectories starting from inner regular region | $(N_r)$ | = | 9975 |
| NUMBER of trajectories starting from the quasiperiodic region for the resonance (8,1) | $(N_{qp,1})$ | = | 0 |
| NUMBER of regular trajectories | $(\bar{N} = N_r + N_{qp,1})$ | = | 9975 |
| NUMBER of trajectories starting from the stochastic region $R_0$ | $(N_0)$ | = | 25 |
| NUMBER of trajectories starting from the stochastic region $R_1$ | $(N_1)$ | = | 0 |
| NUMBER of trajectories starting from the stochastic region $R_2$ | $(N_2)$ | = | 0 |
| FRACTION of regular trajectories | $(\bar{n} = \bar{N}/N)$ | = | 99.75% |
| FRACTION of trajectories starting from the stochastic region $R_0$ | $(n_0 = N_0/N)$ | = | 0.25% |
| FRACTION of trajectories starting from the stochastic region $R_1$ | $(n_1 = N_1/N)$ | = | 0.0% |
| FRACTION of trajectories starting from the stochastic region $R_2$ | $(n_2 = N_2/N)$ | = | 0.0% |

state ($j = 0$, $v = 2$) at ambient temperature, one is led to conclude that IR photodesorption has often to be thermally stimulated. In fact, our results show that a selective effect such as IR-RMVP, i.e., predesorption, is a very weak one for $CH_3F$ desorbing from NaCl.

## ACKNOWLEDGMENTS

Computational support of the CNR's Progetto Finalizzato Sistemi Informatici e Calcolo Parallelo is greatly appreciated. We are also grateful to Z. W. Gortel for a very careful reading of the manuscript.

## APPENDIX A

Consider a Poincaré section in the phase space $(y, p_y)$ for the ERSD system. Let $\mathcal{H}_{(n_i,m_i)}$ be the unstable cycle associated with the $i$th resonances $(n_i, m_i)$. Call $\mathcal{S}_{(n_i,m_i)}$ the separatrix of $\mathcal{H}_{(n_i,m_i)}$ without homoclinic oscillations. Let $\mathcal{R}_{(n_i,m_i)}$ be the closed polygonal line obtained connecting any couple of adjacent hyperbolic points of $\mathcal{H}_{(n_i,m_i)}$ by a segment. Define $\sigma_i(n_i, m_i)$ as the closed curve constituted by that part of $\mathcal{S}_{(n_i,m_i)}$ lying outside $\mathcal{R}_{(n_i,m_i)}$ as the dividing surface in our problem. Following Refs. 17 and 18, we generally subdivide the phase space in each Poincaré section as follows: $B_1$, the inner regular region constituted by the invariant tori plus the islands; $B_2$, a region $R_0$ in between the regular one and the first closed curve just defined, say $\sigma_0(n_0, m_0)$; $B_3$, $i$ regions $R_i$ defined in between $\sigma_{i-1}(n_{i-1}, m_{i-1})$ and $\sigma_i(n_i, m_i)$ with $1 \leq i \leq s-1$; $B_4$, the region $R_s$ outside $\sigma_{s-1}(n_{s-1}, m_{s-1})$ and inside the desorption separatrix without the homoclinic oscillations.

## APPENDIX B

Consider a 2D conservative Hamiltonian system with two degrees of freedom, described by the following Hamiltonian:

$$H(x, y, p_x, p_y) = H_0 + \varepsilon H'. \tag{B1}$$

In Eq. (B1) $H_0$ is an integrable Hamiltonian and $\varepsilon H'$ a nonlinear perturbation to it. Let $\mathcal{T}$ be the mapping induced by the Hamiltonian $H$, which describes the time evolution of the system on the Poincaré section $(y, p_y)$ defined for $x = \bar{x}$. In the following only the dynamics of the system on such a Poincaré section will be considered. Label $\alpha$ a noninvariant closed curve under $\mathcal{T}$ ($\mathcal{T}\alpha \neq \alpha$) and let $R_\alpha$ be the stochastic region surrounded by $\alpha$. Following Bensimon and Kadanoff,[15] the transport rate of the points belonging to $R_\alpha$ through $\alpha$ can be defined as

$$\kappa(\mathcal{T}, R_\alpha) = \frac{L(\mathcal{T}, R_\alpha)}{\Omega, (R_\alpha)}, \tag{B2}$$

where $\Omega(R_\alpha)$ is the area of the region $R_\alpha$, and

$$L(\mathcal{T}, R_\alpha) = \Omega\left[\mathcal{T}(R_\alpha) \cap R_\alpha^c\right]. \tag{B3}$$

In Eq. (B3) $R_\alpha^c$ is the complement of $R_\alpha$. In Fig. 8 the dashed shaded region is $L(\mathcal{T}, R_\alpha)$.

We wish to extend the definition (B3) to the case where the dynamics of the system is not fully stochastic. Assume that within $R_\alpha$ there is a region $R_\beta$, limited by at least one invariant torus under $\mathcal{T}$ ($\mathcal{T}\beta = \beta$). In general, within it there may be invariant tori not destroyed by the perturbation, while the resonant invariant tori are destroyed by the nonlinear coupling $\varepsilon H'$ and replaced by an even number of fixed points (elliptic and hyperbolic points). The separatrix joining the hyperbolic points is usually enclosed by a stochastic layer. However, being such a stochastic layer surrounded by invariant tori, it cannot contribute to $L$, nor can the regular portion of the region $R_\beta$. In conclusion, $L$ is only determined by the points of $R_\alpha$ between $\alpha$ and the invariant torus $\beta$. We call such a region $\rho$ (the dotted area in Fig. 8), and define the transport rate through $\alpha$, where $R_\alpha$ is not completely stochastic, as

$$\kappa(\mathcal{T}, R_\alpha) = \frac{L(\mathcal{T}, \rho)}{\Omega(\rho)}, \tag{B4}$$

where $L(\mathcal{T}, \rho) = \Omega\left[\mathcal{T}(\rho) \cap R_\alpha^c\right]$.

The difference between Eq. (B2) and Eq. (B4) essentially lies in the denominator. At first sight one could say that being $\Omega(\rho) < \Omega(R_\alpha)$ the definition (B4) contradicts intuition, since the transport rate apparently increases when the regular region surrounded by $R_\alpha$ is larger. In practice, however, as we have verified, the numerator decreases faster as soon as the area of the stochastic region becomes smaller. The parameter $\kappa$ is a dimensionless rate. To convert this rate to the units defined in Ref. 14 we need the time phase-space average between two crossings of any trajectory through the surface of section. In the case of the ERSD model parametrized in such a way as to describe $CH_3F$-NaCl, this quantity coincides with the period of the harmonic oscillator $T_H$. In conclusion, the transport rate out of the region $\rho$ is

$$\lambda_\rho = \frac{\kappa(\mathcal{T}, \rho)}{T_H}. \tag{B5}$$

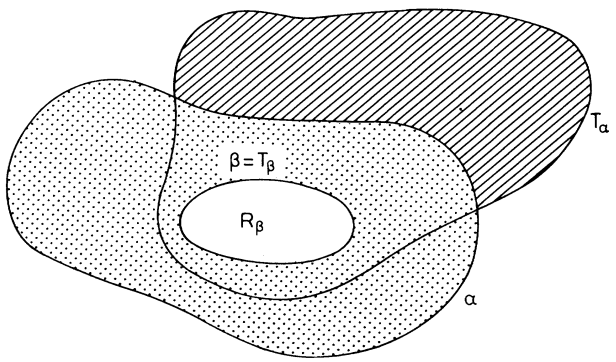


FIG. 8. Flux transport through a noninvariant curve $\alpha$: $R_\beta$, regular region surrounded by an invariant curve $\beta$; the dotted area is the stochastic region surrounded by $\alpha$; the dashed area is the flux out stochastic region.

The transport rate into the region $\rho$ can be trivially defined by substituting in Eq. (B4) $\Omega(\rho)$ with $\Omega(\rho^c - R_\beta)$.

## APPENDIX C

Although the mathematical details of the derivation will be discussed more rigorously elsewhere,[27] it is worthwhile to summarize the main steps of the procedure, which allows one to calculate the hyperbolic point of the cycle $(n,m)$ and its eigenvectors. Consider the Poincaré section describing the phase space of a 2D conservative system and let $\mathbf{Q}$ be a hyperbolic point of the system, relative to a cycle associated to a resonance $(n,m)$. Introduce a polar frame with origin $\mathbf{Q}$ and consider a circle centered at $\mathbf{Q}$ with radius $r$. The length of $r$ has to be smaller than the distance between $\mathbf{Q}$ and the nearest elliptic point, which can be trivially visualized by the phase-space portrait. The points $\boldsymbol{\xi}$ on such a circle are defined by the vector

$$\boldsymbol{\xi}(\theta) \equiv r \begin{pmatrix} \cos\theta \\ \sin\theta \end{pmatrix}. \tag{C1}$$

Define the following function:

$$\begin{aligned} D_r^2(\theta) &= |(\mathcal{T}_{\mathrm{ERSD}}^{n+1} - I)\boldsymbol{\xi}(\theta)|^2 \\ &\equiv |S\boldsymbol{\xi}(\theta)|^2 = \boldsymbol{\xi}^T(\theta)(S^T S)\boldsymbol{\xi}(\theta), \end{aligned} \tag{C2}$$

where $\mathcal{T}_{\mathrm{ERSD}}$ is the mapping describing the dynamics of the system on the Poincaré section for the ERSD model ($\boldsymbol{\xi}^T$ and $S^T$ are the transposed vector and the transposed matrix). The function $D_r^2(\theta)$ gives the squared distance, between a point $\boldsymbol{\xi}$ and its image under the $(n+1)$th iterate of the mapping $\mathcal{T}_{\mathrm{ERSD}}$, in the neighborhood of $\mathbf{Q}$, and displays two maxima of equal magnitude and two minima equal to zero, for $0 \le \theta \le 2\pi$.

Take now a circle centered at $\mathbf{R} \neq \mathbf{Q}$ and call $d$ the distance between $\mathbf{Q}$ and $\mathbf{R}$. Then the function $D_r^2(\theta)$ shows two different behaviors according to the ratio $d/r$, for $0 \le \theta \le 2\pi$: $\mathrm{c}_1$, if $d/r < 1$, $D_r^2(\theta)$ still shows two maxima and two minima but the magnitude of the two maxima (minima) is different; $\mathrm{c}_2$, if $d/r > 1$, $D_r^2(\theta)$ has only one maximum and one minimum. As already pointed out, the main difficulty of the TTHS for the ERSD model parametrized to describe photodesorption of $CH_3F$-NaCl is to locate the hyperbolic points $\mathbf{Q}$ of an unstable cycle $(n,m)$ with the utmost accuracy. So we have worked out the following procedure in order to obtain one of them.

($\mathbf{C_1}$) From the structure of the Poincaré section $(y,p_y)$ for $x = x_0$, we can make a reasonable guess $\bar{\mathbf{Q}} \equiv (\bar{y},\bar{p}_y)$ for the coordinates of the hyperbolic point. In the frame of reference centered at $\bar{\mathbf{Q}}$, call $(r_Q,\theta_Q)$ the polar coordinates of $\mathbf{Q}$. Obviously if $\mathbf{Q} = \bar{\mathbf{Q}}$, $D_{r_Q}^2(\theta_Q) = 0$, since any hyperbolic point $\mathbf{Q}$ is a stationary one for the system.

($\mathbf{C_2}$) If not, choose a circle centered at $\bar{\mathbf{Q}}$ of radius $r$ such that the function $D_r^2(\theta)$ fulfills the property $\mathbf{c_2}$. This is because we want an expression for $D_r^2(\theta)$ with only one minimum within the interval $0 \le \theta \le 2\pi$ (see the forthcoming point $\mathbf{C_4}$). Then subdivide the circle into $N$ arcs. The extrema of each arc locate $N+1$ points on the Poincaré section of coordinates $y_i = r\cos\theta_i$ and $p_{y_i} = r\sin\theta_i$, with $i = 1,\ldots,N+1$. They define $N+1$ different initial conditions for the ERSD system.

($\mathbf{C_3}$) Integrate the equations of motion up to the $(n+1)$th intersection of the corresponding $N+1$ trajectories with the Poincaré section, say $[\mathcal{T}_{\mathrm{ERSD}}^{n+1}(y_i), \mathcal{T}_{\mathrm{ERSD}}^{n+1}(p_{y_i})]$.

($\mathbf{C_4}$) Calculate

$$\begin{aligned} D_r^2(\theta_i) &\equiv D_r^2(y_i,p_{y_i}) \\ &= \{[\mathcal{T}_{\mathrm{ERSD}}^{n+1}(y_i) - y_i]^2 + [\mathcal{T}_{\mathrm{ERSD}}^{n+1}(p_{y_i}) - p_{y_i}]^2\}. \end{aligned} \tag{C3}$$

We determine the coordinates of the minimum as a function of $\theta_i$ and use its coordinates as a new guess $\mathbf{Q}'$ for the position of $\mathbf{Q}$. Then we choose a new (smaller) $r$ satisfying $\mathbf{c_2}$.

($\mathbf{C_5}$) We iterate the method until $D_r^2(\theta)$ calculated from Eq. (C3) reaches zero with the required numerical accuracy. So we can determine the coordinates of $\mathbf{Q}$ with the necessary accuracy [see point (ii) in Sec. III].

This procedure does not require any extrapolation of the mapping $\mathcal{T}_{\mathrm{ERSD}}$ and smoothly converges to the hyperbolic point $\mathbf{Q}$.

Once we have computed the coordinates of $\mathbf{Q}$, we need its eigenvectors to construct the stable and unstable branches associated with it. Although the mapping $\mathcal{T}_{\mathrm{ERSD}}$ is a nonanalytic one, in the neighborhood of $\mathbf{Q}$ it can be safely considered as being its linearized form $\mathcal{T}_{0,\mathrm{ERSD}}$.

Following Ref. 25 we can use its $(n+1)$th iterate and look for its eigenvectors. We can write

$$\mathcal{T}_{0,\mathrm{ERSD}}^{n+1} = \begin{pmatrix} a_{11} & a_{12} \\ a_{12} & a_{22} \end{pmatrix}. \tag{C4}$$

We look for a transformation to calculate the matrix elements of $\mathcal{T}_{0,\mathrm{ERSD}}^{n+1}$ from those of $S_0^T S_0$,

$$S_0^T S_0 = \begin{pmatrix} b_{11} & b_{12} \\ b_{12} & b_{22} \end{pmatrix} = \begin{bmatrix} (a_{11}-1)^2 + a_{21}^2 & (a_{11}-1)a_{12} + a_{21}(a_{22}-1) \\ (a_{11}-1)a_{12} + a_{21}(a_{22}-1) & a_{12}^2 + (a_{22}-1)^2 \end{bmatrix}. \tag{C5}$$

Substituting Eq. (C5) in Eq. (C2) and using Eq. (C1), one obtains

$$b_{11}\sin^2\theta + b_{12}\sin 2\theta + b_{22}\cos^2\theta = \frac{D_r^2(\theta)}{r^2}. \tag{C6}$$

The matrix elements $b_{ij}$ of $(S_0)^T S_0$ can be obtained by choosing three different values of theta, $\theta_k$, $k = 1,2,3$, which locate a particular point belonging to the circle of center $\mathbf{Q}$. Integrating the three corresponding trajectories, we can evaluate $D_r^2(\theta_k)$ for each $k$. A simple way to calculate the matrix elements of $\mathcal{T}_{0,\mathrm{ERSD}}^{n+1}$ from those of $S_0^T S_0$ is supplied

by the following transformation:

$$\begin{array}{ll} (a_{11}-1)=p_1\cos\omega_1, & a_{21}=p_2\sin\omega_2, \\ a_{12}=p_2\cos\omega_2, & (a_{22}-1)=p_2\sin\omega_2. \end{array} \tag{C7}$$

Substituting Eq. (C7) in Eq. (C5), the new variables satisfy

$$p_1=\sqrt{b_{11}}, \tag{C8}$$

$$p_2=\sqrt{b_{22}}, \tag{C9}$$

$$\omega_1^{\pm}=2\arctan\left[\frac{p_2\pm\{(p_2U)^2+(p_1-p_2W)^2-(p_1p_2W)^2\}^{\frac{1}{2}}}{(p_1-p_2W)+p_1p_2W}\right], \tag{C10}$$

$$\omega_2^{\pm}=\omega_1^{\pm}-\arccos(U), \tag{C11}$$

with

$$U=\frac{b_{12}}{p_1p_2} \tag{C12}$$

and

$$W=\sqrt{1-U^2}. \tag{C13}$$

The transformation (C5)–(C13) defines two linear mappings, $\mathcal{T}_{0,\mathrm{ERSD}}^{n+1,(\pm)}$ associated with the function $D_r^2(\theta)$. So given $S_0^T S_0$ by integrating the equations of motion for one initial condition very close to the hyperbolic point **Q**, we can select the right mapping and hence obtain the correct eigenvectors **v**. Propagating in time the trajectories along either eigenvector from adjacent hyperbolic points, one can construct the stable and unstable branches of the separatrix together with its homoclinic oscillations (see Fig. 6).


[1] X.L. Zhou, X.Y. Zhou, and J.M. White, Surf. Sci. Rep. **13**, 77 (1991).
[2] R.D. Ramsier and J.T. Yates, Jr., Surf. Sci. Rep. **12**, 247 (1991).
[3] P. Avouris and R.E. Walkup, Annu. Rev. Phys. Chem. **40**, 173 (1989).
[4] G.P Brivio and T.B. Grimley, Surf. Sci. Rep. **17**, 1 (1993).
[5] Z.W. Gortel, Surf. Sci. **231**, 193 (1990).
[6] J. Heidberg, H. Stein, E. Riehl, Z. Szilagyi, and H. Weiss, Surf. Sci. **158**, 553 (1985).
[7] T.J. Chuang, H. Seki, and I. Hussla, Surf. Sci. **158**, 525 (1985).
[8] P.M. Ferm and G.M. McClelland, J. Chem. Phys. **98**, 700 (1993).
[9] P. Piercy, Z.W. Gortel, and H.J. Kreuzer, in *Advances in Multi-Photon Processes and Spectroscopy*, edited by S.H. Lin (World Scientific, Singapore, 1987), Vol. 3, pp. 105–335.
[10] Y. Guan, J.T. Mukerman, and T. Uzer, J. Chem. Phys. **93**, 4400 (1990).
[11] D. Lucas and G.E. Ewing, Chem. Phys. **58**, 385 (1981).
[12] J.W. Gadzuk, J. Chem. Phys. **86**, 5196 (1987).
[13] S. Holloway and J.W. Gadzuk, J. Chem. Phys. **82**, 5203 (1985).
[14] G.P. Brivio and Z.W. Gortel, Surf. Sci. **261**, 359 (1992).
[15] D. Bensimon and L.P. Kadanoff, Physica D **13**, 82 (1984).
[16] R.S. MacKay, J.D. Meiss and I.C. Percival, Physica D **13**, 55 (1984).
[17] M.J. Davis, J. Chem. Phys. **83**, 1016 (1985).
[18] M.J. Davis and S.K. Gray, J. Chem. Phys. **84**, 5389 (1986).
[19] Z.W. Gortel, H.J. Kreuzer, P. Piercy, and R. Teshima, Phys. Rev. B **27**, 5066 (1983).
[20] S.K. Gray, S.A. Rice, and D.W. Noid, J. Chem. Phys. **84**, 3745 (1986).
[21] J.W. Gadzuk, J. Electron Spectrosc. Relat. Phenom. **45**, 371 (1987).
[22] V. Balasubramanian, N. Sathyamurthy, and J.W. Gadzuk, Surf. Sci. **221**, L741 (1989).
[23] V. Balasubramanian, A. Bahel, I.P. Dubey, N. Sathyamurthy, and J.W. Gadzuk, J. Phys. Chem. **96**, 7870 (1992).
[24] A.J. Lichtenberg and M.A. Lieberman, *Regular and Stochastic Motion* (Springer-Verlag, New York, 1983), p. 168.
[25] A.J. Lichtenberg and M.A. Lieberman, *Regular and Stochastic Motion* (Springer-Verlag, New York, 1983), p. 170.
[26] A.J. Lichtenberg and M.A. Lieberman, *Regular and Stochastic Motion* (Springer-Verlag, New York, 1983), p. 241.
[27] M. Torri and G.P. Brivio (unpublished).